PCCP

ROYAL SOCIETY OF CHEMISTRY

PAPER

View Article Online
View Journal | View Issue

Cite this: *Phys. Chem. Chem. Phys.*, 2025, **27**, 20577

Liquid–liquid equilibrium and modelling insight: molecular interaction analysis of water + methanol + dimethyl carbonate + 1-ethyl-3-methylimidazolium methanesulfonate ternary systems

Juho-Pekka Laakso,* Behnaz Asadzadeh, Petri Uusi-Kyyny and Ville Alopaeus

In this work, ternary liquid–liquid equilibrium (LLE) was measured for water (H_2O) + dimethyl carbonate (DMC) + 1-ethyl-3-methylimidazolium ([Emim][$MeSO_3$]) and methanol (MeOH) + DMC + [Emim][$MeSO_3$] mixtures at 293.15 K at atmospheric pressure. LLEs were modelled utilizing COnductor-like Screening MOdel for Real Solvents (COSMO-RS) and non-random two-liquid (NRTL) models. COSMO-RS was utilized to provide insight into interactions at molecular level through chemical potentials corresponding to the sigma profile and predicted excess enthalpies. The nature of COSMO-RS accuracy was qualitative, while NRTL had an accuracy of 0.013 and 0.030 root mean square deviation for LLE of H_2O + DMC + [Emim][$MeSO_3$] and MeOH + DMC + [Emim][$MeSO_3$] mixtures, respectively. Hydrogen bonding behavior explained favorable [Emim][$MeSO_3$]–H_2O and –MeOH interactions. These interactions might be mainly due to strong hydrogen bond donor interaction between [$MeSO_3$] anion–H_2O and –MeOH. The unfavorable [Emim][$MeSO_3$]–DMC interaction was explained by electrostatic repulsion, possibly arising from repulsion between [$MeSO_3$] anion and DMC oxygens.

Received 12th June 2025,
Accepted 2nd September 2025

DOI: 10.1039/d5cp02239h

rsc.li/pccp

1. Introduction

Utilizing carbon dioxide (CO_2) to synthesize valuable chemicals offers a promising strategy for cost-effective atmospheric CO_2 emissions removal, which mitigates the impact of CO_2 on the climate while obtaining essential chemicals.[1] Dimethyl carbonate (DMC) is a promising environmentally friendly chemical used *e.g.* as a solvent, battery electrolyte, and fuel additive.[2] Traditionally, DMC has been synthesized *via* methanol (MeOH) phosgenation, transesterification, and oxidative carbonylation. These synthesis routes present drawbacks, such as using toxic phosgene or a high risk of explosion.[3] Besides these routes, CO_2 and MeOH can be used to synthesize DMC, which is an environmentally sustainable and safe method. However, this synthesis is limited by thermodynamics,[3] while equilibrium conversion can be as low as 1%.[4] This highlights the significance of strategies for improving equilibrium conversion. One promising approach is to use H_2O absorbents for *in situ* H_2O trapping.[5]

Ionic liquids (ILs) are a class of salts that melt at temperature under 100 °C. These are generally claimed to be non-volatile, non-flammable, and air and H_2O-stable.[6] One significant advantage of ILs is the ability to tailor their properties by modifying the ion combinations from which they are formed. With at least one million possible ion combinations,[7] ILs offer vast potential for customizing their properties. The tunable nature of ILs have been employed in the extraction and separation of bioactive compound,[8] where the hydrophilicity or hydrophobicity can be adjusted by varying the cation–anion combination. ILs have also been employed in integrated CO_2 capture and conversion,[9] where ILs can not only dissolve CO_2 but, also act as a catalyst simultaneously.

1-Ethyl-3-methylimidazolium methanesulfonate ([Emim][$MeSO_3$]) has interesting interaction with H_2O, MeOH and DMC. Excess enthalpy[10] and infinite dilution activity coefficient[11,12] measurements indicate strong [Emim][$MeSO_3$]–H_2O and slightly weaker [Emim][$MeSO_3$]–MeOH attractive interaction while [Emim][$MeSO_3$]–DMC interaction is repulsive. Gas drying is a possible practical application of [Emim][$MeSO_3$] due to experimentally determined low activity coefficient, low viscosity, and high thermal stability.[13]

We investigated liquid–liquid equilibrium (LLE) behavior of the H_2O/MeOH + DMC + [Emim][$MeSO_3$] ternary system, since LLE data can be helpful in designing solvents for reactive systems.[14] It allows one to estimate whether the mixture has

Department of Chemical and Metallurgical Engineering, Aalto University, School of Chemical Engineering, P.O. Box 11000, FI-00076 Aalto, Finland.
E-mail: juho-pekka.laakso@aalto.fi

more than one liquid phase and how reactants and products will distribute in the liquid phases. Thus, it allows one to design these systems to improve the desired yield of the product. This approach has been used in esterification reactions, where IL was used as a solvent to improve conversion of reaction.[15] Phase split into two liquid phases also imply conditions where interactions between the components are strong, allowing for more definite conclusions regarding molecular level phenomena.

Experimental phase equilibrium regarding components relevant to this study has been studied in the literature. Experimental LLE study has been conducted for MeOH + DMC + H_2O mixture at different temperatures.[16] LLE data have been measured for MeOH + DMC + IL systems using a few ILs. Measured ILs include imidazolium-based cation with hydrogen sulfate,[17] dimethyl, and diethyl phosphonium anion.[18] The LLE of MeOH and DMC involving hydroxyethyl ammonium cation with different carboxylate anions has been measured.[19] Also, binary and quaternary vapor–liquid equilibrium, including MeOH + DMC + H_2O + [Emim][$MeSO_3$] has been measured previously.[20]

Non-random two liquids model (NRTL)[21] is a popular for phase equilibrium modeling. The NRTL model is an activity coefficient-based model with a correlative nature. It uses experimental data for regression binary interaction parameters and can accurately estimate phase equilibrium. NRTL has been successfully used to model the LLE of MeOH + DMC + IL systems.[17,18] COnductor like screening MOdel for real solvents (COSMO-RS)[22] is an activity coefficient-based model, which uses only structural information calculated *via* quantum chemistry. A key advantage of COSMO-RS is the ability to give phase equilibrium predictions without experimental data.[23] This makes COSMO-RS suitable for solvent screening.[24] However, COSMO-RS is capable of predicting LLE in general, while a comprehensive analysis of these predictions has been made for binary and ternary mixtures, including ILs.[25–28]

COSMO-RS can give insight into molecular interactions by predicting the chemical potential corresponding to the sigma profile ($\mu(\sigma)$). This chemical potential quantifies favorable and unfavorable interactions that compounds have with different polarities. Thus, one can estimate the component's affinity towards hydrogen bond donor (HBA), non-polar, and hydrogen bond acceptor (HBA) characteristics.[23] Interaction within mixtures can be evaluated by excess enthalpy (H^E). COSMO-RS is able not only to predict H^E but also to quantify the contribution of electrostatic (H^E(MF)), hydrogen bonding (H^E(HB)), and van der Waals (H^E(vdW)) interactions to H^E, thus giving insight into the interaction present in mixtures. A study on the COSMO-RS ability to predict H^E for a wide range of components with ILs indicate that the accuracy of these predictions is generally in good agreement with experiments.[29]

In this work, we measured the LLE of ternary mixtures including DMC, [Emim][$MeSO_3$], and either H_2O/MeOH. As far as we know, this is the first time these LLEs have been experimentally measured. NRTL and COSMO-RS were used to model the LLE behavior in those mixtures. Insight into interactions at the molecular level was studied using COSMO-RS, which was used to explain the LLE behavior. The novelty of this work is not only new LLE experimental data for DMC + H_2O + [Emim][$MeSO_3$] and DMC + MeOH + [Emim][$MeSO_3$] mixtures but also the insight into interactions at the molecular level that can be used to explain the behavior of these LLE. The experimental procedure is provided in Section 2 while modeling approaches are in Section 3. The experimental and modeling results are in Section 4, and the conclusions are presented in Section 5.

2. Experimental

2.1 Materials

The compounds utilized in this study are shown in Table 1. Compounds were acquired from Sigma-Aldrich. The H_2O content in [Emim][$MeSO_3$] was determined using the Karl–Fischer titrator. Milli-Q ultrapure H_2O was produced using the H_2O purification system (Direct-Q 5 UV) and applied to prepare the mixtures.

2.2 Apparatus and procedure

2.2.1 Determination of binodal curves. We used the cloud-point method[30] to determine the binodal curves. We used a 50 cm^3 glass cell to determinate the values of binodal curves. Around this cell, H_2O at 293.15 K was circulated in a surrounding jacket made of glass a Lauda E200 thermostat (Germany) was utilized for regulating temperature with a $u(T)$ = 0.2 K uncertainty. The formation of two liquid phases was detected by the mixture becoming turbid after titrated with DMC and MeOH to a predefined concentration of (H_2O + [Emim][$MeSO_3$]) and (DMC + [Emim][$MeSO_3$]) solution. We measured the mass composition for each binodal measurement, where titration caused turbidity, utilizing analytical balance which has uncertainty of $u(m)$ = 0.002 g.

2.2.2 Determination of tie lines. We performed the LLE measurements at atmospheric pressure by using the glass

Table 1 Chemicals used in this work

Chemicals	CAS number	Supplier	Purity	H_2O content mass fraction	Purification method
1-Ethyl-3-methylimidazolium methanesulfonate	145022-45-3	Merck	≥98.8	0.0090	Vacuum drying
Dimethyl carbonate	616-38-6	Merck	≥99.0	Undetectable	Molecular sieves
2-Propanol	67-63-0	Honeywell	≥99.9	Undetectable	Molecular sieves
Methanol	67-56-1	Merck	≥99.9	0.0001	Molecular sieves
H_2O	7732-18-5		Type I, k: 0.05 μS cm^{-1} at 298 K		

apparatus detailed by Männistö *et al.*[31] as detailed in our previous work.[32] To determine tie lines, we prepared feed samples by mixing needed amount of (MeOH + DMC + [Emim][$MeSO_3$]) and (DMC + [Emim][$MeSO_3$] + H_2O) in the apparatus at fixed temperature utilizing the thermostat (Model: Lauda E200, Germany). The inlet and outlet H_2O temperatures were measured utilizing calibrated Pt-100 probes connected to an ASL CTR-2000-24 thermometer with $u(T)$ = 0.2 K uncertainty. The samples underwent thorough mixing and were given at least 72 hours to split into two distinct liquid phases. We assumed that equilibrium was achieved once the difference in mass fraction was below 0.0001 for two repeated measurements. After two clear phases separated, samples from each liquid phases were obtained utilizing a Hamilton sample-lock syringe. The collected samples were transformed into vials preloaded with the 2-propanol. After separating the two phases, the DMC, MeOH, and H_2O concentrations were determined using Agilent 7890B gas chromatography (GC). In addition, the concentration of [Emim][$MeSO_3$] can be estimated using mass balance. Sampling and analysis for each solution were performed at least three times after equilibrium had been achieved. The configuration for Agilent 7890B GC is shown in Table S1. We calibrated the GC utilizing mixtures with measured masses of 2-propanol with MeOH, DMC, and H_2O. We computed the response factor (F_i) according eqn (1).

$$F_i = F_{\text{std}} \cdot \frac{A_{\text{std}}}{A_i} \cdot \frac{m_i}{m_{\text{std}}} \tag{1}$$

where A_i is the peak area for component i, A_{std} is the peak area for 2-propanol, which is used as a solvent, m_i, and m_{std} are the masses for component i and the solvent, respectively. The response factor of 2-propanol (F_{std}) was set to 1. While analyzing the samples, the relative response factor between the component and the solvent peak area described eqn (1) was not considered. Mass fractions of [Emim][$MeSO_3$] for each sample were determined by subtracting the mass of other components from the total mass. In few measurements, this subtraction resulted in small negative mass fractions. Thus, in these measurements the composition was calculated by setting mass fraction of [Emim][$MeSO_3$] to zero.

2.3 Uncertainty of measurement

An essential aspect of experimental work is determining the measurement uncertainty since this reflects the exact knowledge of the measurement value. Guidelines for the determination of measurement uncertainties are explained in the literature.[33,34] This can be calculated in different ways, such as standard uncertainty (u), combined standard uncertainty (u_c) eqn (2), and expanded standard uncertainty (U) eqn (3). In this work, expanded standard uncertainties with 95% level of confidence (coverage factor of k = 2) were computed for experimental data. The equations used for expanded uncertainty calculations are shown in eqn (S1)–(S4).

$$u_c = \sqrt{\sum_{i=1}^{N} \left(\frac{\partial f}{\partial x_i} u_{x_i} \right)^2} \tag{2}$$

$$U = k u_c \tag{3}$$

where u_c = combined uncertainty, f = function, x_i = input variable, k = coverage factor and U = expanded uncertainty.

3. Phase equilibria modelling

3.1 Criteria of phase equilibrium

The thermodynamic criteria for phase equilibrium are fulfilled when fugacity (f) of each component in any two co-existing phases is equal, as shown in eqn (4). Under assumption of ideal behavior in the vapor phase, the criteria for the vapor–liquid equilibrium can be described as in eqn (5). The liquid–liquid equilibrium is typically expressed by using activity coefficients (γ). Thus, eqn (4) can be written as eqn (6) when the definition of activity coefficient is used instead of fugacities.[35]

$$f_i^{\text{I}} = f_i^{\text{II}} \tag{4}$$

$$y_i P_{\text{total}} = x_i \gamma_i P_i \tag{5}$$

$$x_i^{\text{I}} \gamma_i^{\text{I}} = x_i^{\text{II}} \gamma_i^{\text{II}} \tag{6}$$

Where f_i = fugacity of component i, y_i = vapor phase mole fraction of component i, x_i = liquid phase mole fraction of component i, γ_i = activity coefficient of component i, P_{total} = total pressure of the system, and P_i = vapor pressure of pure component i. In this work, the vapor pressure of pure components was obtained from extended Antoine correlations eqn (S5). Parameters for extended Antoine correlation for MeOH, DMC, and H_2O were obtained from ASPEN software, while these parameters were regressed for [Emim][$MeSO_3$]. The resulting regression is shown in Fig. S1, while the parameters are in Table S2.

3.2 Non-random two liquids (NRTL)

The non-random two liquids (NRTL)[21] is a popular model base on activity coefficients that has been successfully used to model phase equilibria of mixtures involving ILs.[17,18] The NRTL uses two parameters per binary system, which describe the interaction between these two molecules. These parameters are regressed from phase equilibrium data. In addition, NRTL has so-called ''non-randomness'' parameter (α), which is set to a constant value for each component pair or regressed from data. The general form of the NRTL model is shown in eqn (7). In this work, NRTL modeling was performed in ASPEN V14, which uses NRTL correlation as defined in eqn (7)–(12).[36]

$$\ln \gamma_i = \frac{\sum_j x_j \tau_{ji} G_{ji}}{\sum_k x_k G_{ki}} + \sum_j \frac{x_j G_{ij}}{\sum_k x_k G_{kj}} \left(\tau_{ij} - \frac{\sum_m x_m \tau_{mj} G_{mj}}{\sum_k x_k G_{kj}} \right) \tag{7}$$

$$G_{ij} = \exp(-\alpha_{ij} \tau_{ij}) \tag{8}$$

$$\tau_{ij} = a_{ij} + \frac{b_{ij}}{T} + e_{ij} \ln(T) + f_{ij} T \tag{9}$$

$$\alpha_{ij} = c_{ij} + d_{ij}(T - 273.15\ \text{K}) \tag{10}$$

$$\tau_{ii} = 0 \quad (11)$$

$$G_{ii} = 1 \quad (12)$$

The parameters for the NRTL model are typically regressed from binary phase equilibria data, and in the absence of such data, parameters can be obtained from ternary phase equilibrium data. In this work, we regressed NRTL parameters using binary and ternary phase equilibrium data while NRTL parameters fitted to binary data were used as a initial guesses. This way, parameters can describe binary and ternary systems. We used an objective function called "maximum likelihood", which is described in detail in the ASPEN V14 help.[36] During the regression, we fixed the α parameters according to the literature.[21] Specifically, α was fixed to 0.2 for binary mixtures which showed LLE behavior, and to 0.3 otherwise. We also evaluated the consistency of NRTL parameters to describe LLE according to the literature.[37,38]

3.3 COnductor-like Screening Model for Real Solvent (COSMO-RS)

The COnductor-like Screening Model for Real Solvent (COSMO-RS) is a quantum chemistry approach for predicting phase equilibria.[22,24,39] The main advantage of COSMO-RS is its predictive ability. The details of COSMO-RS theory are presented in the literature.[23] In COSMO-RS, the polarity of molecules in the fluid-like phase is calculated around the molecule's surface, and this polarity is represented as charged surface segments that interact pairwise. The phase equilibria are calculated from statistical thermodynamics using these segments. These segments are represented as charge density, which is represented in a histogram called "σ-profile" Fig. 1. The COSMO-RS model is shown in eqn (13)–(19).[40]

The σ-profile can be calculated for mixtures, as shown in eqn (13).

$$P_s(\sigma) = \frac{\sum_i x_i P^{X_i}(\sigma)}{\sum_i x_i A^{x_i}} \quad (13)$$

Electrostatics (E_{misfit}) and hydrogen bonding (E_{HB}) molecular interactions are described by using interaction surface segments σ and σ' or $\sigma_{acceptor}$ and σ_{donor}. The van der Waals interaction is described in more approximate way. The energetic contribution of these interactions are calculated as showed in eqn (14)–(16).

$$E_{misfit}(\sigma,\sigma') = a_{eff}\frac{\alpha'}{2}(\sigma+\sigma')^2 \quad (14)$$

$$E_{vdW} = a_{eff}\left(\tau_{vdW} + \tau'_{vdW}\right) \quad (15)$$

$$E_{HB} = a_{eff}c_{HB}\min(0;\min(0;\sigma_{donor}+\sigma_{HB})\max(0;\sigma_{acceptor}+\sigma_{HB})) \quad (16)$$

where a_{eff} = effective contact area, α' = an interaction parameter, c_{HB} = the hydrogen bond strength, τ_{vdW} = an elements specific vdW interaction parameter, σ_{HB} = the cut of hydrogen bonding. The chemical potential is a key thermodynamic quantity

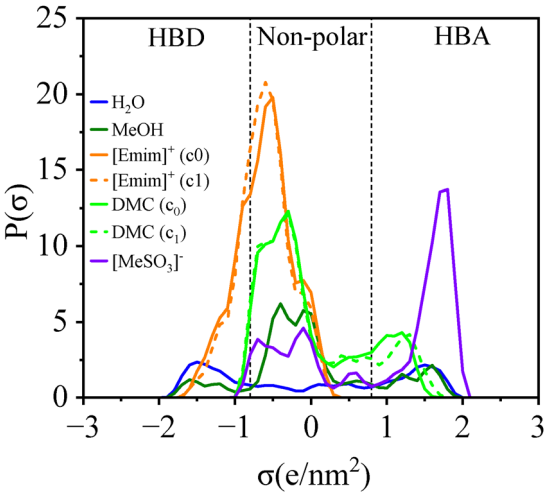

Fig. 1 The unnormalized σ-profiles for H_2O, MeOH, [Emim]–cation, DMC, and [$MeSO_3$]–anion. The c_0 and c_1 are lowest and second lowest energy conformation of molecule.

regarding phase equilibrium which can be calculated for the solvent from $p_s(\sigma)$ according to eqn (17).

$$\mu_s(\sigma) = -\frac{RT}{a_{eff}}\ln\left[\int P_s(\sigma')\exp\left(\frac{1}{RT}(a_{eff}\mu_s(\sigma') - E_{misfit}(\sigma,\sigma') - E_{HB}(\sigma,\sigma'))\right)d\sigma'\right] \quad (17)$$

The $\mu_s(\sigma)$, referred to as "σ-potential", describes the affinity of the solvent S towards a given surface polarity σ. Interactions are modelled pairwise, thus the term ($P_s(\sigma')$) describes the distribution of surface charge polarities that come into contact with surface charge polarities of solvent ($P_s(\sigma)$). The $\mu_s(\sigma')$ is the chemical potential of contacting surface segments σ'. The factor a_{eff} represents the surface area of contacting segments. The E_{misfit} term represents electrostatic misfit energy between a pair of surface polarities of σ and σ'. This gives the contribution of the local interaction between σ and σ' surface polarities originated from electrostatics. The E_{HB} accounts for the additional stabilization due to hydrogen bonding, which arises when two strongly and opposite surface polarities contact and is not included in E_{misfit}. Thus, the $\mu_s(\sigma)$ is computed taking into account the chemical potential of the environment, the distribution of surface polarities and pairwise electrostatic and hydrogen-bond interactions between surface polarities. The van der Waals interaction can be added to the solutions reference energy. Pseudo chemical potential of compound X_i can be determined by integrating of $\mu_s(\sigma)$ over the compound as follows.

$$\mu_S^X = \mu_{C,S}^X + \int P^X(\sigma)\mu_s(\sigma)d\sigma \quad (18)$$

In the eqn (18), the size and shape differences of the molecule in the system and volume dependent term $\mu_{C,S}^X$ are taken account. From σ-potential, the activity coefficient of

arbitrary mixture (γ_S^X) is calculated as in eqn (19).

$$\gamma_S^X = \exp\left\{\frac{\mu_S^X - \mu_X^X}{RT}\right\} \quad (19)$$

Where μ_X^X is the reference state of the pure compound.

Excess enthalpy of a fluid mixture (H^E) can be predicted using COSMO-RS *via* summing the contribution of each component as shown in eqn (20)–(22).[29,41]

$$H^E = \sum x_i H_i^E = \sum x_i (H_i - H_i^0) \quad (20)$$

where H_i^E is excess enthalpy of component i, x_i is mole fraction of component i, H_i is enthalpy of mixture, and H_i^0 enthalpy of pure component i. COSMO-RS calculates H^E from sum of hydrogen bonding (H^E(HB), van der Waals H^E(vdW) and electrostatic contribution (H^E(MF)) to excess enthalpy (eqn (21)) which originates from microscopic interaction energies.

$$H^E = H^E(\text{HB}) + H^E(\text{vdW}) + H^E(\text{MF}) \quad (21)$$

Combining eqn (20) and (21) results eqn (22).

$$H^E = \sum H^E(\text{HB}) + \sum H^E(\text{vdW}) + \sum H^E(\text{MF}) \quad (22)$$

Thus, COSMO-RS predicts excess enthalpy of the mixtures *via* molecular-level interactions present between two different molecules.

In this work, we used COSMOtherm 2024 software[42] with BP_TZVP_24.ctd parameterization, while σ-profiles were obtained from the COSMObase2023 database. We chose to use σ-profiles, which were calculated using the TZVPD-FINE basis set because this predicts LLE more likely compared to the TZVP basis set.[25] Here, the TZVP basis set did not predict LLE in the case of the MeOH + DMC + [Emim][$MeSO_3$] mixture. Also, the COSMOtherm manual stated that the prediction of isobaric VLE for mixtures including ionic liquids is not feasible.[41] However, COSMO-RS predictions for isobaric VLE of H_2O + [Emim][$MeSO_3$] and MeOH + [Emim][$MeSO_3$] resulted in reasonable predictions. Thus, these isobaric predictions were analyzed in this work. Since COSMO-RS modelling was performed by modelling [Emim]-[$MeSO_3$] as individual ions, the composition and activity coefficient of the COSMO-RS predictions should be converted to match the mole fraction definition usually used in the context of ILs.[40,41] We performed this conversion for VLE and LLE predictions.

4. Results and discussion

4.1 Experimental binodal curves and tie line data

Experimental results for LLE for DMC + MeOH + [Emim]-[$MeSO_3$] and DMC + H_2O + [Emim][$MeSO_3$] mixtures at 293.15 K and at atmospheric pressure are shown in Tables 2–4. It was observed that the LLE of DMC + MeOH + [Emim][$MeSO_3$] mixture also included H_2O, which was quantified. However, the mass fraction of H_2O was small enough to consider this a ternary mixture of DMC + MeOH + [Emim][$MeSO_3$]. The composition of one liquid phase was almost pure DMC for both mixtures. However, the composition of the second liquid phase was different. In the DMC + H_2O + [Emim][$MeSO_3$] mixture, the composition of the second phase included a wide range of H_2O and [Emim][$MeSO_3$]. Interestingly, we observed that top and bottom liquid phases were reversed for two measured tie-lines, as shown in Table 4. In the mixture of DMC + MeOH + [Emim]-[$MeSO_3$], the second phase was present only with low mass fraction values for MeOH.

Table 2 Experimental binodal compositions in weight fractions for the DMC + MeOH + [Emim][$MeSO_3$] system at T = 293.15 K and 101 kPa pressure

T/K = 293.15			
DMC + MeOH + [Emim][$MeSO_3$]		DMC + H_2O + [Emim][$MeSO_3$]	
W_{MeOH}	$W_{[Emim][MeSO_3]}$	W_{DMC}	$W_{[Emim][MeSO_3]}$
0.0314	0.0624	0.978	0.013
0.0433	0.11751	0.963	0.007
0.0568	0.1967	0.273	0.713
0.0722	0.2796	0.243	0.729
0.061	0.37941	0.242	0.729
0.0523	0.47013	0.200	0.741
0.031	0.58038	0.194	0.755
0.0249	0.6002	0.184	0.745
		0.142	0.757
		0.137	0.769
		0.120	0.182
		0.118	0.140
		0.118	0.081
		0.115	0.186
		0.115	0.098
		0.106	0.273
		0.105	0.266
		0.095	0.724
		0.081	0.463
		0.080	0.376
		0.079	0.388
		0.076	0.520
		0.067	0.681
		0.065	0.654
		0.065	0.567

Expanded uncertainties are: U_T = 0.4 K, U_P = 20 kPa and U_{wi} = 0.04.

4.2 Modelling results

4.2.1 Binary mixtures. Binary phase equilibrium data were used in this work for NRTL parameter regression. Thus, the ability of NRTL and COSMO-RS was compared as a part of evaluating the modelling ability of both models. Experimental data and average absolute deviation (AAD) of boiling point temperature and liquid phase composition for VLE and LLE systems are shown in Table 5 and illustrated in Fig. 2. The NRTL model accurately described all binary phase equilibrium systems. Accuracy of NRTL was highest for VLE of mixtures not including [Emim][$MeSO_3$], and lowest for mixtures which includes [Emim][$MeSO_3$] and for DMC + H_2O mixture. Similarly, the accuracy of COSMO-RS was highest for non-[Emim][$MeSO_3$] including systems (except for MeOH + DMC mixture), and it has more deviation from experimental data for [Emim][$MeSO_3$] including systems. In the case of the LLE of [Emim][$MeSO_3$] and DMC, the experimental data suggest a marginal decrease in the DMC mole fraction with increasing temperature, although this trend may be affected by measurement uncertainty. In contrast, both NRLT and COSMO-RS predict an opposite trend. For NRTL, the deviation arises from the regression

Table 3 Experimental tie lines compositions in weight fractions for the DMC + MeOH + H_2O + [Emim][$MeSO_3$] mixture at T = 293.15 K and 101 kPa pressure

Feed sample			Top phase: DMC-rich phase				Bottom phase: [Emim][$MeSO_3$]-rich phase			
$W_{[Emim][MeSO_3]}$	W_{MeOH}	W_{DMC}	$W_{[Emim][MeSO_3]}$	W_{MeOH}	W_{DMC}	W_{H_2O}	$W_{[Emim][MeSO_3]}$	W_{MeOH}	W_{DMC}	W_{H_2O}
0.2674	0.0413	0.6912	0	0.0106	0.9855	0.0040	0.3961	0.0558	0.5416	0.0065
0.3220	0.0328	0.6452	0	0.0068	0.9889	0.0043	0.4763	0.0445	0.4725	0.0067
0.3777	0.0288	0.5935	0	0.0052	0.9852	0.0096	0.5066	0.0371	0.4471	0.0091
0.4422	0.0142	0.5435	0.0006	0.0022	0.9920	0.0052	0.5907	0.0180	0.3741	0.0171

Expanded uncertainties are: $U_{w_{MeOH}}$ = 0.004, $U_{w_{DMC}}$ = 0.048, $U_{w_{H_2O}} = 0.019$ and $U_{w_{[Emim][MeSO_3]}} = 0.045$, U_T = 0.4 K, U_P = 20 kPa.

Table 4 Experimental tie lines compositions in weight fractions for the DMC + H_2O + [Emim][$MeSO_3$] mixture at T = 293.15 K and 101 kPa pressure

Feed sample			Top phase: DMC-rich phase			Bottom phase: [Emim][$MeSO_3$]-rich phase		
W_{H_2O}	W_{DMC}	$W_{[Emim][MeSO_3]}$	W_{H_2O}	W_{DMC}	$W_{[Emim][MeSO_3]}$	W_{H_2O}	W_{DMC}	$W_{[Emim][MeSO_3]}$
0.1024	0.4038	0.4938	0.0056	0.9688	0.0256	0.1484	0.0978	0.7538
0.1930	0.4064	0.4006	0.0101	0.9784	0.0114	0.3010	0.0641	0.6350
0.3009	0.4020	0.2971	0.0174	0.9795	0.0031	0.4677	0.0726	0.4597
0.3974	0.4050	0.1976	0.0244	0.9721	0.0035	0.6409	0.0930	0.2661
0.0568	0.3945	0.5486	0.0017	0.9983	0	0.0850	0.1683	0.7467
0.4047	0.3926	0.2027	0.0231	0.9769	0	0.6602	0.0895	0.2503

Feed sample			Top phase: [Emim][$MeSO_3$]-rich phase			Bottom phase: DMC-rich phase		
W_{H_2O}	W_{DMC}	$W_{[Emim][MeSO_3]}$	W_{H_2O}	W_{DMC}	$W_{[Emim][MeSO_3]}$	W_{H_2O}	W_{DMC}	$W_{[Emim][MeSO_3]}$
0.4968	0.3971	0.1061	0.7992	0.1058	0.0950	0.0270	0.9730	0
0.5489	0.3949	0.0562	0.8834	0.1140	0.0026	0.0287	0.9713	0

Expanded uncertainties are $U_{w_{H_2O}} = 0.031$, $U_{w_{DMC}}$ = 0.049, $U_{w_{MeOH}}$ = 0.004 and $U_{w_{[Emim][MeSO_3]}} = 0.046$, U_T = 0.4 K, U_P = 20 kPa.

including all binary and ternary phase equilibria, which provide overall good accuracy despite this in the LLE case. COSMO-RS shows a similar but larger deviation. This model may underestimate repulsive interaction between DMC and [Emim][$MeSO_3$] and over predicts their temperature dependence. Interestingly, COSMO-RS predictions for vapor–liquid–liquid equilibrium (VLLE) of DMC + H_2O mixture were more accurate than NRTL correlation despite parameter regression. Thus, COSMO-RS could give qualitatively and, for a few mixtures, also quantitatively correct predictions for the studied binary systems.

4.2.2 Ternary liquid–liquid equilibria. LLE for DMC + H_2O + [Emim][$MeSO_3$] and DMC + MeOH + [Emim][$MeSO_3$] mixtures are shown in Fig. 3. These were modelled using NRTL and COSMO-RS. The resulting NRTL parameter regression is shown in Table 6. The root mean square deviation (RMSD) of the NRTL model for LLE of DMC + H_2O + [Emim][$MeSO_3$] was 0.013, and for DMC + MeOH + [Emim][$MeSO_3$] was 0.030. Thus, NRTL can model these ternary LLE with high precision. We also estimated the consistency of the NRTL parameters for both mixtures,[37] which are shown in Fig. S2 and S3. According to the software used for this test,[38] these parameters were consistent.

The COSMO-RS predictions were qualitatively accurate as shown in Fig. 3. For the DMC + H_2O + [Emim][$MeSO_3$] mixture, COSMO-RS could predict quantitatively that the composition of one liquid phase is almost pure DMC. COSMO-RS prediction of the second liquid phase in the range of $w_{[Emim][MeSO_3]} < 0.5$ was surprisingly accurate, but in the range of $w_{[Emim][MeSO_3]} > 0.5$, predictions started to deviate from experimental data. Despite this, COSMO-RS has a qualitatively accurate trend for the second liquid phase. COSMO-RS could only predict the ternary LLE of DMC + MeOH + [Emim][$MeSO_3$] mixture when TZVPD-FINE parameterization was used. This parameterization is more likely to predict LLE split than the TZVP parameterization,[25] which might explain this result. COSMO-RS prediction for LLE of DMC + MeOH + [Emim][$MeSO_3$] was similar as in the case of DMC + H_2O + [Emim][$MeSO_3$] mixture. Thus, it could predict the overall shape of the LLE phase envelope, but not LLE behavior quantitatively.

Table 5 The accuracy of NRTL and COSMO-RS for studied binary mixtures

Mixture/system	Type	AAD (K) NRTL	AAD (K) COSMO-RS	Ref.
MeOH + H_2O	VLE	0.6[a]	0.9[a]	43
MeOH + DMC	VLE	0.3[a]	2.2[a]	20
H_2O + [Emim][$MeSO_3$]	VLE	2.7[a]	2.7[a]	20
MeOH + [Emim][$MeSO_3$]	VLE	2.5[a]	6.1[a]	20
DMC + H_2O	VLE	5.6[a]	1.6[a]	44
DMC + H_2O	LLE	0.02[b]	0.07[b]	16
DMC + [Emim][$MeSO_3$]	LLE	0.005[c]	0.3[c]	20

[a] AAD = $\sum |T^{exp} - T^{cal}|/n$. [b] AAD = $\sum |x^{exp}_{DMC} - x^{cal}_{DMC}|/n$. [c] AAD = $\sum |w^{exp}_{DMC} - w^{cal}_{DMC}|/n$.

4.2.3 Molecular interactions. One benefit of COSMO-RS is the ability to describe interactions at the molecular level from the chemical potential corresponding to the σ-profile ($\mu(\sigma)$),[23]

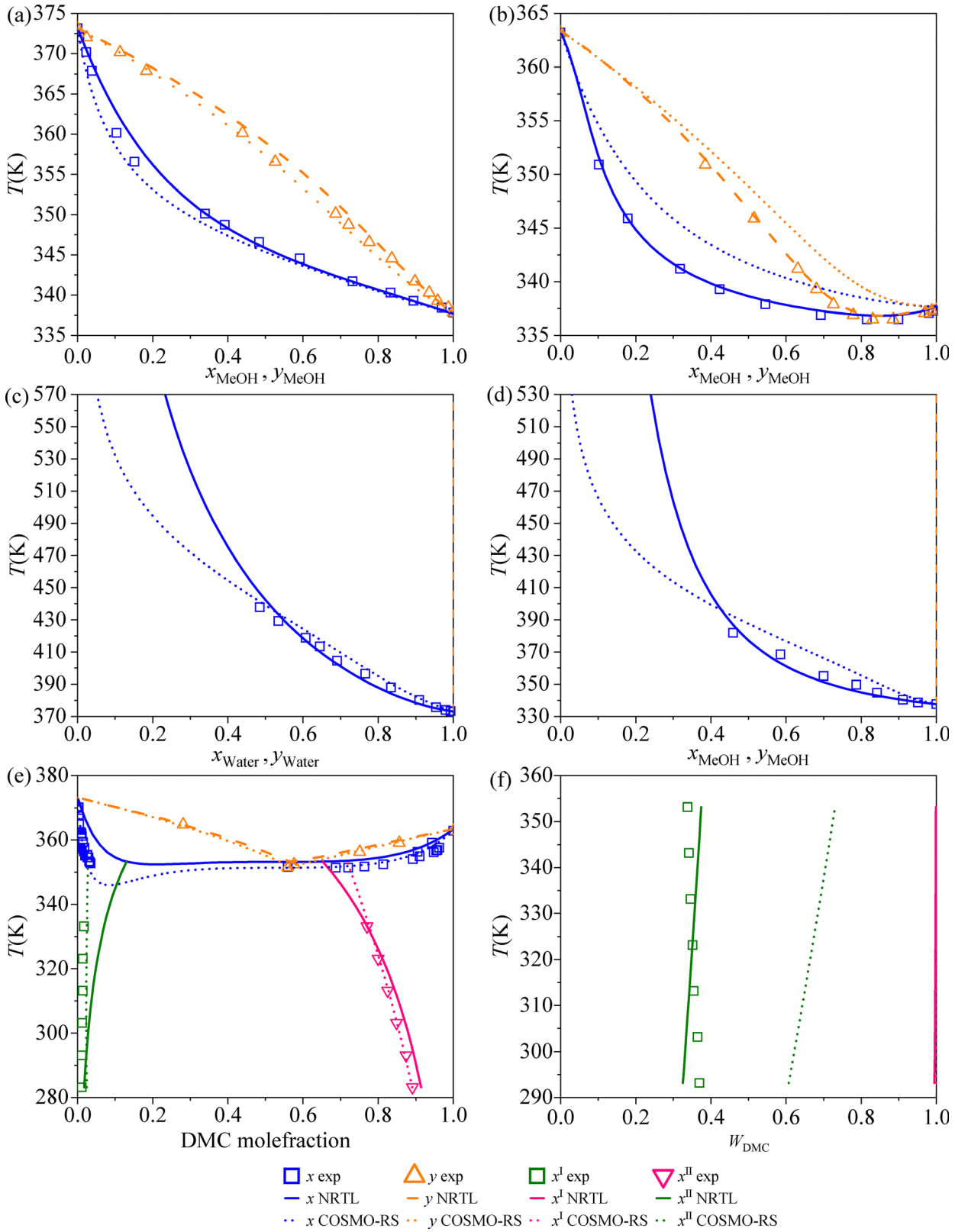

Fig. 2 NRTL and COSMO-RS results for binary systems: (a) MeOH + H_2O, (b) MeOH + DMC, (c) H_2O + [Emim][$MeSO_3$], (d) MeOH + [Emim][$MeSO_3$], (e) DMC + H_2O, and (f) DMC + [Emim][$MeSO_3$].

while interactions within binary mixtures can be estimated from excess enthalpy predictions (H^E).[29] COSMO-RS can predict the contribution of electrostatics (H^E(MF)), hydrogen bonding (H^E(MF)), and van der Waals (H^E(vdW)) interactions to H^E,

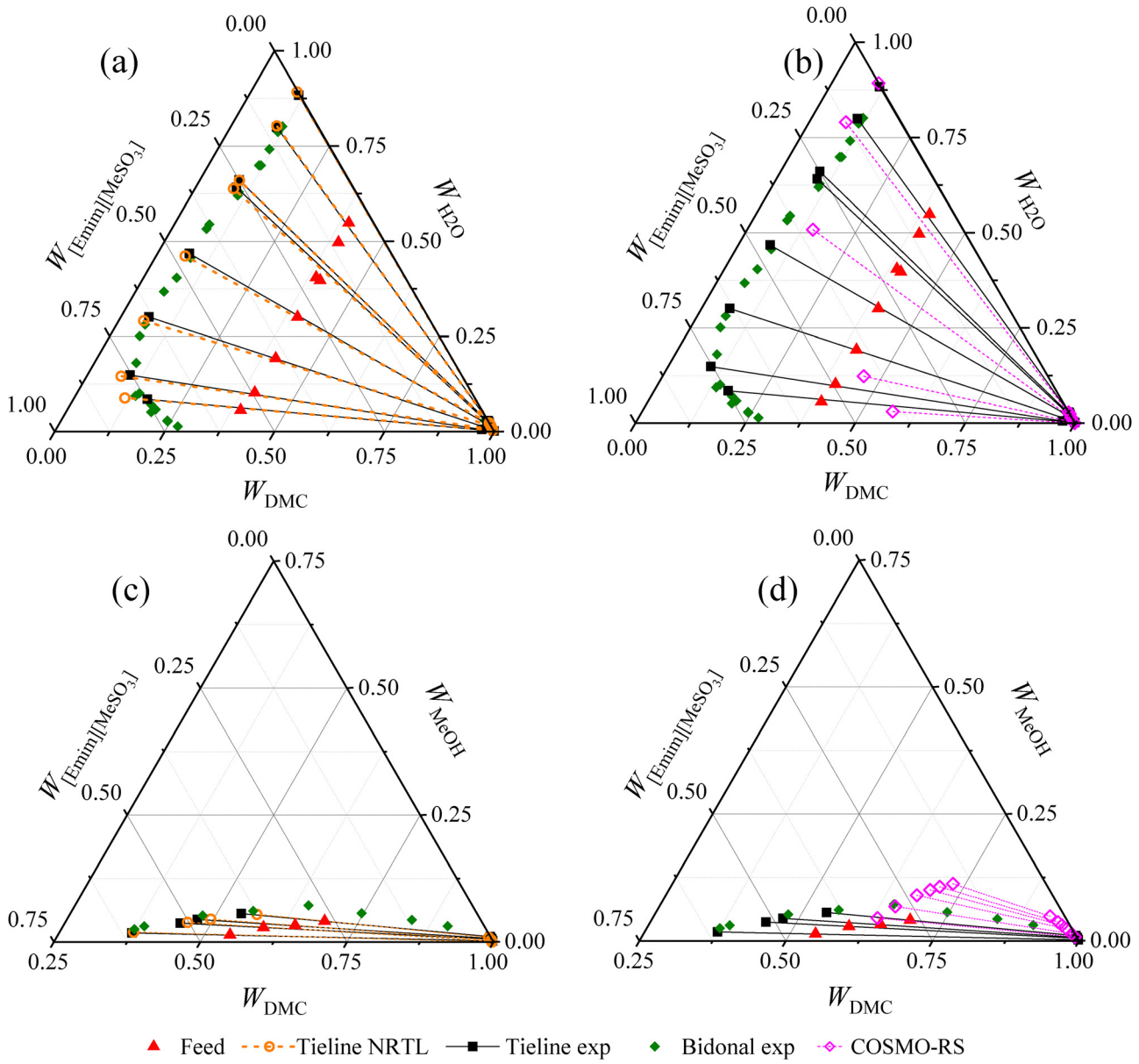

Fig. 3 LLE diagram for DMC + H_2O + [Emim][$MeSO_3$] (a) and (b) and DMC + MeOH + [Emim][$MeSO_3$] (c) and (d) mixtures at 293.15 K and 101.3 kPa. NRTL results are shown in (a) and (c), while COSMO-RS results are in (b) and (d).

giving insight into interactions within mixtures. The screened surface charge (σ-surface) reflects the polarity of a component in a liquid-like phase. The σ-surface for each component investigated in this study is shown in Fig. 4.

Table 6 NRTL parameters for different mixtures in this work, $\tau_{ij} = a_{ij} + b_{ij}/T$ (K)

i–j	a_{ij}	a_{ji}	b_{ij}	b_{ji}	α	RMSD
DMC (1) + H_2O (2) + [Emim][$MeSO_3$] (3)						0.013
1–2	−2.693	−1.448	1072.812	1357.798	0.2	
1–3	15.759	−3.114	−2479.746	490.206	0.2	
2–3	−36.584	1.813	13 258.792	−1533.285	0.3	
DMC (1) + MeOH (2) + [Emim][$MeSO_3$] (3) + H_2O (4)						0.030
1–2	28.112	−30.932	−9298.03	10 722.694	0.3	
1–3	15.759	−3.114	−2479.746	490.206	0.2	
2–3	−21.044	93.461	5295.157	−28 933.843	0.3	
2–4	15.048	−3.978	−4759	1208.97	0.3	

The $\mu(\sigma)$ plots for all studied components are shown in Fig. 5, where $\mu(\sigma)$ describes the affinity of a component or mixture to a specific surface polarity (σ). Values of σ in the range of $\sigma < -0.8$ e/nm^2 describe the affinity towards hydrogen bond donor (HBD). The affinity towards non-polar surface charge is described in the range of -0.8 e/nm^2 $< \sigma <$ 0.8 e/nm^2, while charge $\sigma >$ 0.8 e/nm^2 describes the tendency to interact with hydrogen bond acceptor (HBA). Negative $\mu(\sigma)$ describes a favorable interaction, whereas positive $\mu(\sigma)$ an unfavorable one.

MeOH shows favorable interaction with HBD ($\sigma < -1.75$ e/nm^2), slight repulsion from non-polar to HBA polarity, and favorable interactions again at $\sigma >$ 2 e/nm^2 polarity. This behavior suggests that the oxygen in the MeOH will interact more strongly

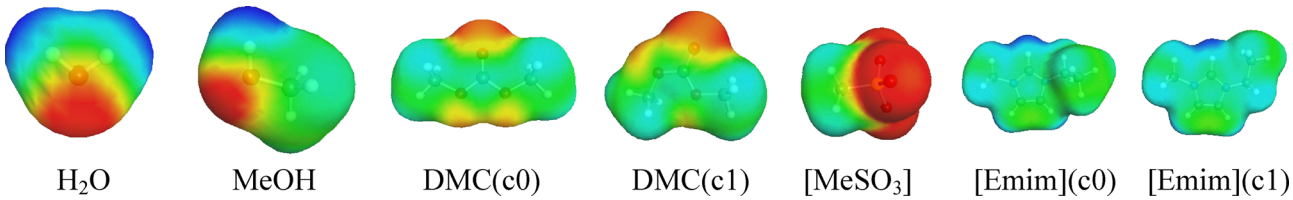

Fig. 4 The σ-surface for H_2O, MeOH, DMC, $[MeSO_3]^-$ and $[Emim]^+$ components. The c_0 and c_1 are lowest and second lowest energy conformation of molecule.

with positively charged species (*e.g.*, polar hydrogens) than with negatively charged ones (*e.g.*, oxygens). The methyl group of MeOH enhances affinity for nonpolar species, as reflected by the lower $\mu(\sigma)$ in the nonpolar region compared to H_2O.

H_2O starts to have increasing affinity for both HBD and HBA at $\sigma < -1.5$ e/nm^2 and $\sigma > 1.25$ e/nm^2 polarity, respectively. The polarity of -1.5 e/nm^2 $< \sigma <$ 1.25 e/nm^2 has more unfavorable interactions than in the case of MeOH. H_2O interacts more strongly with HBA and almost as strongly with HBD than MeOH since H_2O has two polar hydrogens and an electron-rich oxygen. At the same time, the weaker affinity for nonpolar regions is attributed to the lack of nonpolar character.

DMC has favorable interaction with HBD in the range of $\sigma <$ -2 e/nm^2, while DMC has slightly unfavorable interaction over the range -2 e/nm^2 $< \sigma <$ 1 e/nm^2. The magnitude of unfavorable interactions increases in the range of $\sigma >$ 1 e/nm^2. DMC has a similar affinity towards non-polarity as MeOH. The $\mu(\sigma)$ plot can be explained by DMC's electron-rich oxygen in the carbonyl group, which can interact with HBD but has a strong repulsive interaction with HBA. The presence of two methyl groups in DMC might provide a similar affinity to non-polar character as MeOH. Thus, the LLE split between DMC and H_2O may be attributed to H_2O poor ability to interact with non-polar character while DMC has more favorable interaction with non-polar character. Also, H_2O has stronger affinity towards HBD and HBA and DMC has unfavorable affinity towards HBA and less strong affinity towards HBD than H_2O. However, MeOH contains a methyl group that increases its affinity towards non-polar character sufficiently to prevent LLE split between MeOH and DMC.

[Emim] cation has the most unfavorable affinity towards HBD ($\sigma < -0.8$ e/nm^2), while affinity increases almost linearly up to $\sigma = 0$. Affinity to HBA polarity increases dramatically when $\sigma > 2$ e/nm^2. This increase might be due to the positive polarity of the cation, which highly favors HBA and disfavors HBD interactions. [Emim]–cation has a polar hydrogen between two nitrogen atoms as seen in the Fig. 4, which can interact with HBA and thus amplify affinity towards HBA.

$[MeSO_3]$ anion has highly favorable interactions with HBD ($\sigma < -0.8$ e/nm^2). From the HBD region, affinity decreases roughly linearly in the range of $\sigma > -3$ e/nm^2. However, favorable affinity changes to unfavorable in non-polar region, and $[MeSO_3]$ anion has unfavorable interaction with HBA ($\sigma >$ 0.8 e/nm^2). This might be due to the sulfonate group, which has three electron-rich oxygens that can strongly interact with HBD (*e.g.*, polar hydrogens) while disfavoring interactions with HBA (*e.g.*, oxygens). The methyl group might increase slightly affinity towards non-polarity.

The $\mu(\sigma)$ plot of $[Emim][MeSO_3]$ (50 : 50 mixture of [Emim] cation and $[MeSO_3]$ anion) has characteristics from $\mu(\sigma)$ plots of anion and cation. It has favorable interactions with HBD ($\sigma <$ -1.5 e/nm^2) while favorable interactions with HBA occurs in more positively polar characteristics, roughly from $\sigma > 2$ e/nm^2. This might indicate that $[Emim][MeSO_3]$ interacts more easily with HBD, probably through the three electron-rich oxygen atoms in the sulfonate group. Cation needs even more polar

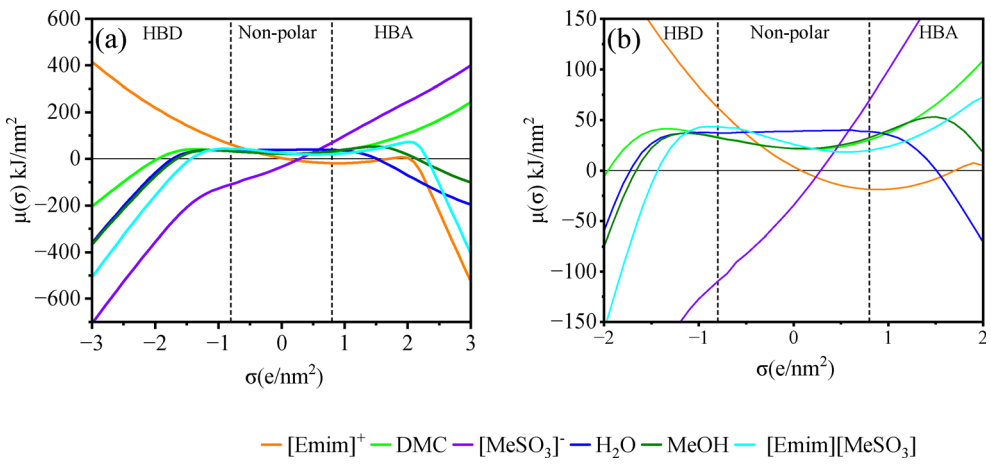

Fig. 5 Chemical potential of the σ-profile segments (a) and zoom in figure (b).

HBA for favorable interaction, indicating that [Emim] cation hydrogens are weakly polar (except one as seen in Fig. 4).

The LLE split between [Emim][$MeSO_3$] and DMC might be due to multiple reasons. First, DMC has more unfavorable interactions with HBA than [Emim][$MeSO_3$]. This might be due to lack of polar hydrogens in DMC while [Emim] cation has at least one polar hydrogen. Second, DMC has more favorable interactions towards non-polar character roughly in the range of $-1 < \sigma < 0$ while DMC has high amount of this polarity according the σ-profile (Fig. 1). [Emim][$MeSO_3$] has strong affinity towards HBD and highly polar HBA. This might indicate that [Emim][$MeSO_3$] interacts strongly with polar hydrogens presents in H_2O and MeOH.

The interactions between molecules in a mixture can be estimated from H^E. These predictions and the LLE envelope for DMC + H_2O + [Emim][$MeSO_3$] are shown in Fig. 6. According to H^E (Fig. 6a), [Emim][$MeSO_3$]–H_2O interaction is attractive while [Emim][$MeSO_3$]–DMC and DMC–H_2O interactions are repulsive. Hydrogen bonding H^E(HB) (Fig. 6c) is the key driver for the interactions. This is attractive to [Emim][$MeSO_3$]–H_2O and repulsive to H_2O–DMC interactions. Electrostatic interactions H^E(MF) (Fig. 6b) explains mainly the repulsive [Emim][$MeSO_3$]–DMC interactions. The H^E(vdW) only makes a minor contribution to these interactions. All interactions that COSMO-RS predicts might not be possible in reality since LLE constrains the compositions that a liquid mixture may have in phase equilibrium conditions. The hypothetical compositions in two liquid phase regions are shown using grey surface in Fig. 6–8.

H^E and the LLE envelope for DMC + MeOH + [Emim][$MeSO_3$] are shown in Fig. 7. This predicts that [Emim][$MeSO_3$]–MeOH has favorable interactions while [Emim][$MeSO_3$]–DMC and MeOH–DMC have repulsive interactions. The interactions are similar with the DMC + H_2O + [Emim][$MeSO_3$] mixture, but the strength of interactions is generally lower. Hydrogen bonding H^E(HB) (Fig. 7c) behavior explains mostly the favorable and unfavorable interactions, while electrostatic behavior (Fig. 7b) has a minor effect on the interactions (except for [Emim][$MeSO_3$]–DMC interactions), and the H^E(vdW) (Fig. 7d) does not have a substantial contribution. Thus, the hydrogen bonding between [Emim][$MeSO_3$]–H_2O or MeOH explains most of these

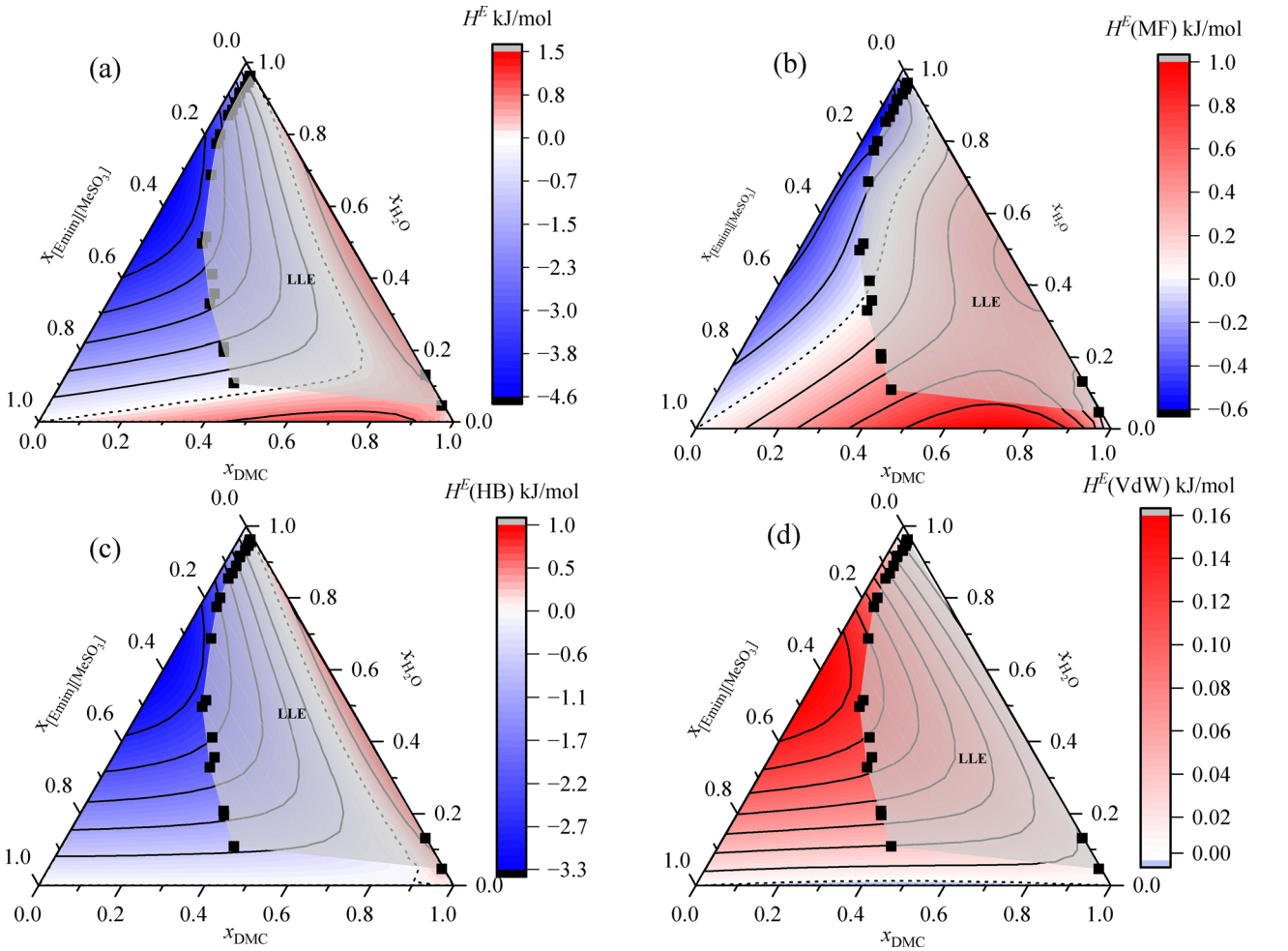

Fig. 6 Contour plot of COSMO-RS predicted excess enthalpy for H_2O + DMC + [Emim][$MeSO_3$] mixture at 293.15 K (a). The contribution of electrostatic (b), hydrogen bonding (c) and van der Waals (d) interactions to excess enthalpy. The dashed line represents 0 excess enthalpy, ■ is experimental binodal measured in this work, grey surface is LLE envelope estimated from binodal measurements.

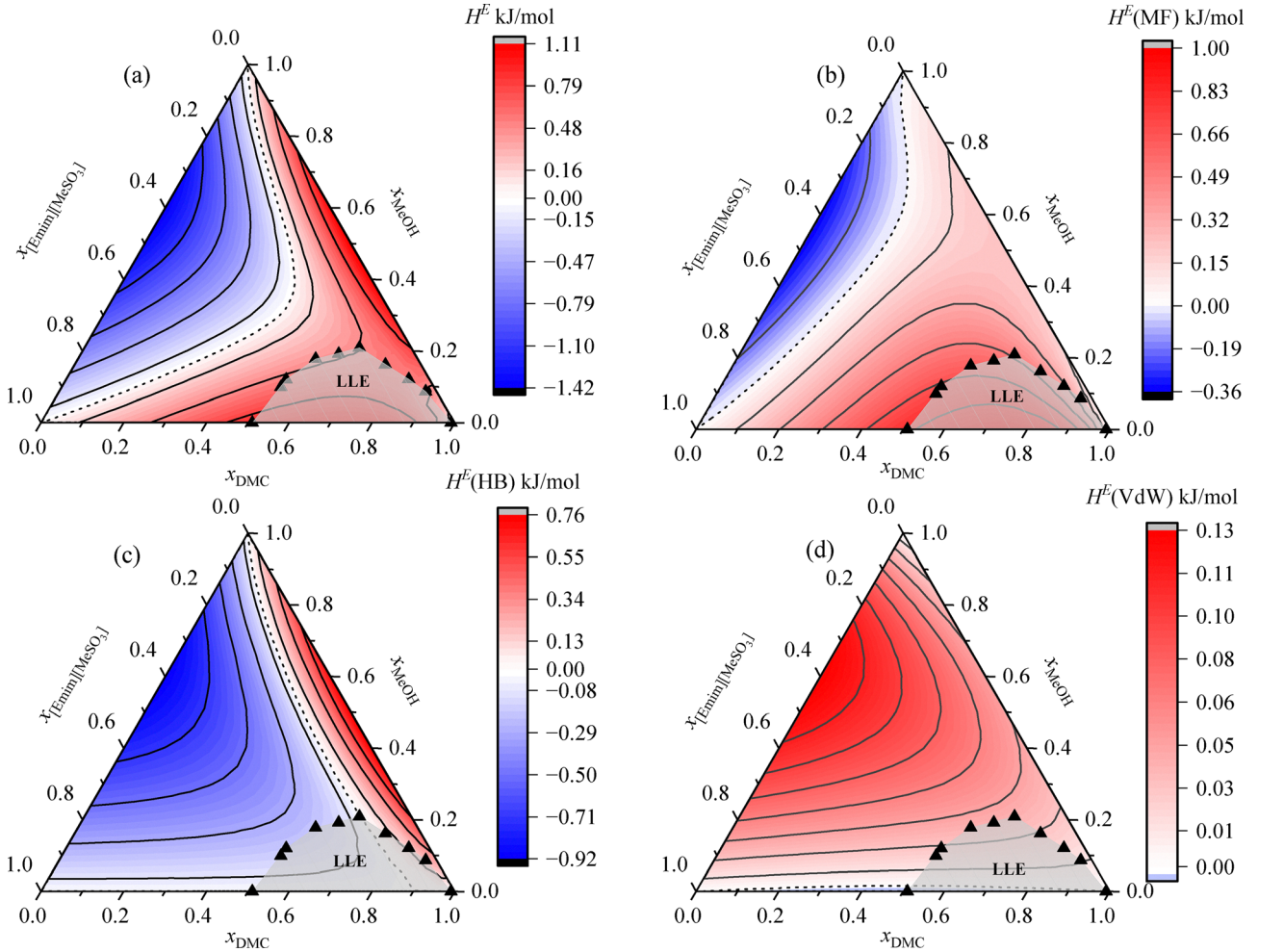

Fig. 7 Contour plot of COSMO-RS predicted excess enthalpy for MeOH + DMC + [Emim][$MeSO_3$] mixture at 293.15 K (a). The contribution of electrostatic (b), hydrogen bonding (c) and van der Waals (d) interactions to excess enthalpy. Dashed line represents 0 excess enthalpy, ▲ is experimental binodal measured in this work, grey surface is LLE envelope estimated from binodal measurements.

interactions, while electrostatic repulsion has a significant contribution to [Emim][$MeSO_3$]–DMC interactions.

The LLE tie lines can be defined from the surface of Gibbs energy of mixing (G^m). The contour plots of G^m for H_2O + DMC + [Emim][$MeSO_3$] and MeOH + DMC + [Emim][$MeSO_3$] systems are displayed in the Fig. 8. For both mixtures, the G^m plots follow the trend from H^E plots. This indicates that the minimum and maximum of the G^m plots originate from the interactions. Minimums are close to molar composition, where interactions are most favorable, and maximums are close to composition, where interactions are unfavorable. Molecular-level interactions can explain this behavior. $\mu(\sigma)$ analysis indicates that H_2O and MeOH can form hydrogen bonding interactions with [Emim][$MeSO_3$]. [Emim][$MeSO_3$] has a strong affinity to HBD (polar hydrogens) and more polar HBA (electron-rich oxygens). At the same time, H_2O and MeOH can provide both HBD and HBA. Stronger interaction with H_2O might originate from two polar hydrogens. DMC has strong repulsion with HBA, while [$MeSO_3$] anion provides electron-rich oxygens, thus explaining the strong repulsion.

5. Conclusion

In this work, ternary LLE of DMC + H_2O + [Emim][$MeSO_3$] and MeOH + DMC + [Emim][$MeSO_3$] was measured at 293.15 K, and measurements were modelled using NRTL and COSMO-RS. Parameters for the NRTL model were regressed utilizing VLE and LLE data from binary mixtures and ternary LLE measurements involving all studied components. COSMO-RS was used to give insight into interaction at the molecular level by calculating the chemical potential corresponding to the σ-profile and predicting excess enthalpies with the contribution of electrostatic, hydrogen bonding, and van der Waals interactions. The Gibbs energy of mixing was predicted to give insight into LLE behavior.

The accuracy of NRTL was higher than COSMO-RS for modelling phase equilibria for binary mixtures, except for VLLE of the DMC + H_2O mixture. NRTL also resulted in higher accuracy for modelling measured ternary LLE mixtures with RMSD values of 0.013 and 0.030 for DMC + H_2O + [Emim]-[$MeSO_3$] and MeOH + DMC + [Emim][$MeSO_3$] mixtures,

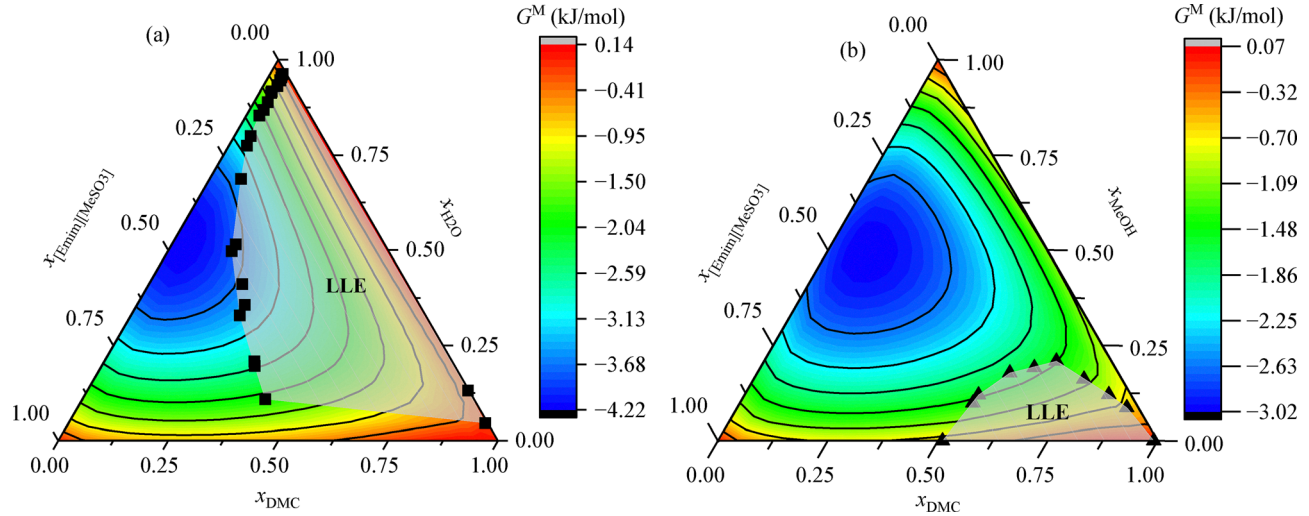

Fig. 8 Contour plot of COSMO-RS predicted Gibbs free energy of mixing for H_2O + DMC + [Emim][$MeSO_3$] (a) and MeOH + DMC + [Emim][$MeSO_3$] (b) mixtures at 293.15 K. ■ is experimental bidonal for H_2O + DMC + [Emim][$MeSO_3$] mixture, ▲ is experimental bidonal for MeOH + DMC + [Emim][$MeSO_3$] mixture, and grey surface is LLE envelope estimated from binodal measurements.

respectively. COSMO-RS was able to predict ternary LLE qualitatively and partly with quantitative accuracy.

The COSMO-RS can provide detailed insight into molecular-level interactions. According to the calculated chemical potential corresponding to the σ-profile, [Emim][$MeSO_3$] has a high affinity towards hydrogen bond donors (HBD) and can have high affinity towards hydrogen bond acceptors (HBA), if polarity is high enough. This can be explained by three electron-rich oxygens in [$MeSO_3$] anion and polar hydrogen in [Emim] cation. DMC exhibits unfavorable interactions with HBA, which can be explained by the lack of polar hydrogens. Both H_2O and MeOH have an affinity towards HBD and HBA, while H_2O has a stronger affinity towards HBA due to its two polar hydrogens. The predicted excess enthalpy indicates that [Emim][$MeSO_3$]–H_2O and [Emim][$MeSO_3$]–MeOH have favorable interactions where the hydrogen bonding contribution is the main driver for interactions. The unfavorable [Emim][$MeSO_3$]–DMC was explained from electrostatic repulsion, which can be connected to repulsion between [$MeSO_3$] anion and DMC oxygens. The calculated Gibbs energy of mixing indicated that these interactions significantly contribute to LLE behavior.

Author contributions

Juho-Pekka Laakso: conceptualization, methodology, investigation, writing – original draft, writing – review & editing. Behnaz Asadzadeh: conceptualization, methodology, validation, writing – original draft, writing – review & editing. Petri Uusi-Kyyny: conceptualization, writing – review & editing, funding, acquisition. Ville Alopaeus: supervision, writing – review & editing.

Conflicts of interest

The authors declare that they have no known competing financial interests or personal relationships that could have appeared to influence the work reported in this paper.

List of symbols

Abbreviations

CAS	Chemical Abstract Service
H_2O	Water
DMC	Dimethyl carbonate
[Emim][$MeSO_3$]	1-Ethyl-3-methylimidazolium methanesulfonate
LLE	Liquid–liquid equilibrium
VLE	Vapor–liquid equilibrium
VLLE	Vapor–liquid–liquid equilibrium
NRTL	Non-random two-liquid
COSMO-RS	Conductor-like Screening Model
CO_2	Carbon dioxide
IL	Ionic liquid
HBA	Hydrogen bonding acceptor
HBD	Hydrogen bonding donor
TZVP	Triple-zeta valence polarization
TZVPD-FINE	Triple-zeta valence with polarization and diffuse functions
RMSD	Root mean square deviation
SO_3	Sulfonate group
AAD	Average absolute deviation

Symbols

F	Response factor
A	Surface area of gas chromatography signal
m	Mass
u_c	Combined uncertainty
U	Combined expanded uncertainty
f	Function
f	Fugacity
y	Mole fraction of vapor phase
x	Mole fraction of liquid phase
γ	Activity coefficient
P	Pressure

n	Number of measurements
α	Non-randomness constant for binary ij interactions in NRTL model
τ, a, b, c, d, e, f, G	Dimensionless interaction parameters in NRTL model
$P(\sigma)$	Sigma profile
A	Surface area of molecule
E_{misfit}	Energy component for misfit interactions
E_{vdW}	Energy component for van der Waals interactions
E_{HB}	Energy component for hydrogen bonding interactions
σ	Surface polarization charge density for a molecule
α'	Effective interaction parameter or scaling factor for damping polar interactions
a_{eff}	Effective surface area in COSMO-RS model
τ_{vdW}	Parameter related to van der Waals damping factor for interactions
c_{HB}	Coefficient representing the strength of hydrogen bonding interactions
σ_{donor}	Charge density or potential related to the hydrogen bond donor site
σ_{HB}	Sigma profile specific to hydrogen bonding interactions
σ_{acceptor}	Charge density or potential related to the hydrogen bond acceptor site
$\mu_s(\sigma)$	Chemical potential specific to surface segment for a solvent
R	Universal gas constant
T	Temperature
$\mu(\sigma)$	Chemical potential specific to surface segment
H^E	Total excess enthalpy
H^E(vdW)	Contribution of van der Waals interaction to excess enthalpy
H^E(MF)	Contribution of misfit (electrostatic) interactions to excess enthalpy
H^E(HB)	Contribution of hydrogen bonding to excess enthalpy
G^m	Gibbs energy of mixing
w	Weight fraction
c_0	Conformation of a molecule structure at the lowest energy level
c_1	Conformation of a molecule structure at a second lowest energy level

Subscript

i	Component i
j	Component j
s	Solvent

Data availability

The data supporting this article have been included as part of the SI. The supplementary information file includes the settings for Agilent 7890B gas chromatography, the equations for calculating the uncertainty of measurements, the vapor pressure correlation for [Emim][$MeSO_3$] and the results of NRTL consistency tests. See DOI: https://doi.org/10.1039/d5cp02239h.

Acknowledgements

This work was supported by Academy of Finland, project "*in situ* equilibrium shifting in CO_2 utilization reactions by novel absorbents (CO_2 shift)" project number 351113. The authors wish to acknowledge CSC – IT Center for Science, Finland, for computational resources.

References

1 C. Hepburn, E. Adlen, J. Beddington, E. A. Carter, S. Fuss, N. Mac Dowell, J. C. Minx, P. Smith and C. K. Williams, The Technological and Economic Prospects for CO2 Utilization and Removal, *Nature*, 2019, **7**, 87–97, DOI: 10.1038/s41586-019-1681-6.

2 M. Zhang, Y. Xu, B. L. Williams, M. Xiao, S. Wang, D. Han, L. Sun and Y. Meng, Catalytic Materials for Direct Synthesis of Dimethyl Carbonate (DMC) from CO2, *J. Cleaner Prod.*, 2021, **279**, 123344, DOI: 10.1016/j.jclepro.2020.123344.

3 A. Raza, M. Ikram, S. Guo, A. Baiker and G. Li, Green Synthesis of Dimethyl Carbonate from CO2 and Methanol: New Strategies and Industrial Perspective, *Adv. Sustainable Syst.*, 2022, **6**(8), 2200087, DOI: 10.1002/adsu.202200087.

4 B. A. V. Santos, C. S. M. Pereira, V. M. T. M. Silva, J. M. Loureiro and A. E. Rodrigues, Kinetic Study for the Direct Synthesis of Dimethyl Carbonate from Methanol and CO2 over CeO2 at High Pressure Conditions, *Appl. Catal., A*, 2013, **455**, 219–226, DOI: 10.1016/j.apcata.2013.02.003.

5 D. Shi, S. Heyte, M. Capron and S. Paul, Catalytic Processes for the Direct Synthesis of Dimethyl Carbonate from CO2and Methanol: A Review, *Green Chem.*, 2022, **24**(3), 1067–1089, DOI: 10.1039/d1gc04093f.

6 Z. Lei, B. Chen, Y. M. Koo and D. R. Macfarlane, Introduction: Ionic Liquids, *Chem. Rev.*, 2017, **117**(10), 6633–6635, DOI: 10.1021/acs.chemrev.7b00246.

7 N. V. Plechkova and K. R. Seddon, Applications of Ionic Liquids in the Chemical Industry, *Chem. Soc. Rev.*, 2008, **37**(1), 123–150, DOI: 10.1039/b006677j.

8 S. P. M. Ventura, F. A. e Silva, M. V. Quental, D. Mondal, M. G. Freire and J. A. P. Coutinho, Ionic-Liquid-Mediated Extraction and Separation Processes for Bioactive Compounds: Past, Present, and Future Trends, *Chem. Rev.*, 2017, **24**, 6984–7052, DOI: 10.1021/acs.chemrev.6b00550.

9 Y. Chen and T. Mu, Conversion of CO2 to Value-Added Products Mediated by Ionic Liquids, *Green Chem.*, 2019, **21**(10), 2544–2574, DOI: 10.1039/c9gc00827f.

10 L. E. Ficke and J. F. Brennecke, Interactions of Ionic Liquids and Water, *J. Phys. Chem. B*, 2010, **114**(32), 10496–10501, DOI: 10.1021/jp1012736.

11 U. Domańska and M. Królikowski, Measurements of Activity Coefficients at Infinite Dilution for Organic Solutes and

Water in the Ionic Liquid 1-Ethyl-3-Methylimidazolium Methanesulfonate, *J. Chem. Thermodyn.*, 2012, **54**, 20–27, DOI: 10.1016/j.jct.2012.03.005.

12 A. Blahut, M. Sobota, V. Dohnal and P. Vrbka, Activity Coefficients at Infinite Dilution of Organic Solutes in the Ionic Liquid 1-Ethyl-3-Methylimidazolium Methanesulfonate, *Fluid Phase Equilib.*, 2010, **299**(2), 198–206, DOI: 10.1016/j.fluid.2010.10.008.

13 M. Krannich, F. Heym and A. Jess, Characterization of Six Hygroscopic Ionic Liquids with Regard to Their Suitability for Gas Dehydration: Density, Viscosity, Thermal and Oxidative Stability, Vapor Pressure, Diffusion Coefficient, and Activity Coefficient of Water, *J. Chem. Eng. Data*, 2016, **61**(3), 1162–1176, DOI: 10.1021/acs.jced.5b00806.

14 A. Rathgeb, A. Palmtag, S. Kaminski and A. Jupke, Design of Extractive Reaction Systems, *Chem. Ing. Tech.*, 2019, **91**(12), 1766–1776, DOI: 10.1002/cite.201900163.

15 Q. Zeng, H. Qin, H. Cheng, L. Chen and Z. Qi, Development of a Reactive Extraction Process for Isobutyl Isobutyrate Formation Intensified by Bifunctional Ionic Liquid, *Chem. Eng. Sci.: X*, 2019, **1**, 100001, DOI: 10.1016/j.cesx.2018.100001.

16 J. de la Torre, A. Cháfer, A. Berna and R. Muñoz, Liquid-Liquid Equlibria of the System Dimethyl Carbonate + Methanol + Water at Different Temperatures, *Fluid Phase Equilib.*, 2006, **247**(1–2), 40–46, DOI: 10.1016/j.fluid.2006.05.029.

17 G. Wen, X. Geng, W. Bai, Y. Wang and J. Gao, Ternary Liquid-Liquid Equilibria for Systems Containing (Dimethyl Carbonate or Methyl Acetate + methanol + 1-Methylmidazole Hydrogen Sulfate) at 298.15 K and 318.15 K, *J. Chem. Thermodyn.*, 2018, **121**, 49–54, DOI: 10.1016/j.jct.2018.02.012.

18 F. Cai, J. J. Ibrahim, L. Gao, R. Wei and G. Xiao, A Study on the Liquid-Liquid Equilibrium of 1-Alkyl-3-Methylimidazolium Dialkylphosphate with Methanol and Dimethyl Carbonate, *Fluid Phase Equilib.*, 2014, **382**, 254–259, DOI: 10.1016/j.fluid.2014.09.016.

19 X. Wang, Y. Cui, Y. Song, Y. Liu, J. Zhang, S. Chen, L. Dong and X. Zhang, Studies on the Prediction and Extraction of Methanol and Dimethyl Carbonate by Hydroxyl Ammonium Ionic Liquids, *Molecules*, 2023, **28**(5), 2312, DOI: 10.3390/molecules28052312.

20 J. P. Laakso, B. Asadzadeh, P. Uusi-Kyyny, X. Liang, G. M. Kontogeorgis and V. Alopaeus, Experimental and Cubic Plus Association Equation of State Modelling Study of Phase Equilibria of 1-Ethyl-3-Methylimidazolium Methanesulfonate + Methanol + Dimethyl Carbonate + Water Binary and Quaternary Mixtures: The Role of Ionic Liquids Vapor Pressure in Modelling, *J. Mol. Liq.*, 2025, **422**, 126775, DOI: 10.1016/j.molliq.2024.126775.

21 H. Renon and J. M. Prausnitz, Local Compositions in Thermodynamic Excess Functions for Liquid Mixtures, *AIChE J.*, 1968, **14**, 135–144.

22 A. Klamt, Conductor-like Screening Model for Real Solvents: A New Approach to the Quantitative Calculation of Solvation Phenomena, *J. Phys. Chem.*, 1995, **99**(7), 2224–2235, DOI: 10.1021/j100007a062.

23 A. Klamt, *COSMO-RS: From Quantum Chemistry to Fluid Phase Thermodynamics and Drug Design*, 2005.

24 F. Eckert and A. Klamt, Fast Solvent Screening *via* Quantum Chemistry: The COSMO-RS Approach, *AIChE J.*, 2002, **48**, 369–385, DOI: 10.1002/aic.690480220.

25 K. Paduszyński and M. Królikowska, Extensive Evaluation of Performance of the COSMO-RS Approach in Capturing Liquid-Liquid Equilibria of Binary Mixtures of Ionic Liquids with Molecular Compounds, *Ind. Eng. Chem. Res.*, 2020, **59**(25), 11851–11863, DOI: 10.1021/acs.iecr.0c00449.

26 K. Paduszyński, Extensive Evaluation of the Conductor-like Screening Model for Real Solvents Method in Predicting Liquid-Liquid Equilibria in Ternary Systems of Ionic Liquids with Molecular Compounds, *J. Phys. Chem. B*, 2018, **122**(14), 4016–4028, DOI: 10.1021/acs.jpcb.7b12115.

27 A. R. Ferreira, M. G. Freire, J. C. Ribeiro, F. M. Lopes, J. G. Crespo and J. A. P. Coutinho, Overview of the Liquid-Liquid Equilibria of Ternary Systems Composed of Ionic Liquid and Aromatic and Aliphatic Hydrocarbons, and Their Modeling by COSMO-RS, *Ind. Eng. Chem. Res.*, 2012, **51**(8), 3483–3507, DOI: 10.1021/ie2025322.

28 Y. Lyu, J. F. Brennecke and M. A. Stadtherr, Review of Recent Aromatic-Aliphatic-Ionic Liquid Ternary Liquid- Liquid Equilibria and Their Modeling by COSMO-RS, *Ind. Eng. Chem. Res.*, 2020, **59**(19), 8871–8893, DOI: 10.1021/acs.iecr.0c00581.

29 K. A. Kurnia and J. A. P. Coutinho, Overview of the Excess Enthalpies of the Binary Mixtures Composed of Molecular Solvents and Ionic Liquids and Their Modeling Using COSMO-RS, *Ind. Eng. Chem. Res.*, 2013, **52**(38), 13862–13874, DOI: 10.1021/ie4017682.

30 R. Dahal, P. Uusi-Kyyny, J. P. Pokki and V. Alopaeus, Liquid – Liquid Equilibria in Binary and Ternary Systems of Phenol + Hydrocarbons (n–Dodecane or n–Hexadecane) and Water + Phenol + Hydrocarbons (n–Dodecane or n–Hexadecane) at Temperatures between 298K and 353K, *Fluid Phase Equilib.*, 2022, **556**, 113402, DOI: 10.1016/j.fluid.2022.113402.

31 M. Männistö, J. P. Pokki, A. Creati, A. Voisin, A. Zaitseva and V. Alopaeus, Ternary and Binary LLE Measurements for Solvent (4-Methyl-2-Pentanone and 2-Methyl-2-Butanol) + Furfural + Water between 298 and 401 K, *J. Chem. Eng. Data*, 2016, **61**(2), 903–911, DOI: 10.1021/acs.jced.5b00738.

32 B. Asadzadeh, M. Saad, P. Uusi-Kyyny and V. Alopaeus, Reactive Extraction of Levulinic Acid from Aqueous Solutions Using Trioctylamine with Diluents 2-Ethyl-1-Hexanol, 4-Methylpentan-2-One, and Isoamyl Alcohol, *J. Chem. Eng. Data*, 2023, **69**, 3566–3572, DOI: 10.1021/acs.jced.3c00309.

33 Working Group 1 of the Joint Committee for Guides in Metrology (JCGM/WG 1), JCGM 100 2008 GUM 1995 with Minor Correction. Evaluation of Measurement Data Guide to the Expression of Uncertainty in Measurement, 2008. https://www.bipm.org/utils/common/documents/jcgm/JCGM_100_2008_E.pdf (accessed 2024-08-05).

34 D. B. Hibbert, Uncertainties in the Measurement of Solubility – A Tutorial, *J. Chem. Thermodyn.*, 2019, **133**, 152–160, DOI: 10.1016/j.jct.2019.02.007.

35 S. Sandler, *Chemical and Engineering Thermodynamics*, Wiley, 5th edn, 2017.

36 AspenTech, Aspen Plus, Version 14, (2022). **https://www.aspentech.com**.
37 A. Marcilla, J. A. Reyes-Labarta and M. M. Olaya, Should We Trust All the Published LLE Correlation Parameters in Phase Equilibria? Necessity of Their Assessment Prior to Publication, *Fluid Phase Equilib.*, 2017, **433**, 243–252, DOI: **10.1016/j.fluid.2016.11.009**.
38 J. A. Reyes-Labarta, *Graphical User Interface (GUI) for the Representation of GM Surfaces (Using the NRTL Model) and Curves, Including Tie-Lines and Hessian Matrix. Institutional Repository of the University of Alicante (RUA)*. **https://hdl.handle.net/10045/51725** (accessed 2025-05-19).
39 A. Klamt, V. Jonas, T. Bu and J. C. W. Lohrenz, Refinement and Parametrization of COSMO-RS, *J. Phys. Chem. A*, 1998, **102**(26), 5074–5085.
40 M. Diedenhofen and A. Klamt, COSMO-RS as a Tool for Property Prediction of IL Mixtures-A Review, *Fluid Phase Equilib.*, 2010, **294**(1–2), 31–38, DOI: **10.1016/j.fluid.2010.02.002**.
41 BIOVIA, *Dassault Systèmes, Reference Manual*, Dassault Systèmes, San Diego, 2023.
42 BIOVIA, *Dassault Systèmes, COSMOtherm2024*, Dassault Systèmes, San Diego, 2024. **https://www.3ds.com/products/biovia**.
43 C. Yang, S. Ma and X. Yin, Organic Salt Effect of Tetramethylammonium Bicarbonate on the Vapor-Liquid Equilibrium of the Methanol-Water System, *J. Chem. Eng. Data*, 2011, **56**(10), 3747–3751, DOI: **10.1021/je200341c**.
44 S. Camy, J.-S. Pic, E. Badens and J.-S. Condoret, Fluid Phase Equilibria of the Reacting Mixture in the Dimethyl Carbonate Synthesis from Supercritical CO2, *J. Supercrit. Fluids*, 2003, **25**(1), 19–32.